Heliyon 10 (2024) e28722

Contents lists available at ScienceDirect

Heliyon

journal homepage: www.cell.com/heliyon

Research article

Radiomics analysis of intratumoral and different peritumoral regions from multiparametric MRI for evaluating HER2 status of breast cancer: A comparative study

Jing Zhou [a,2], Xuan Yu [a,2], Qingxia Wu [b], Yaping Wu [a], Cong Fu [a], Yunxia Wang [a], Menglu Hai [c], Hongna Tan [a,**], Meiyun Wang [a,*,1]

[a] Department of Medical Imaging, Henan Provincial People's Hospital & People's Hospital of Zhengzhou University & Imaging Diagnosis of Neurological Diseases and Research Laboratory of Henan Province, Zhengzhou, 450003, Henan Province, China
[b] Beijing United Imaging Research Institute of Intelligent Imaging & United Imaging Intelligence (Beijing) Co., Ltd., Beijing, 100089, China
[c] Department of Radiology, The Affiliated Cancer Hospital of Zhengzhou University & Henan Cancer Hospital, Zhengzhou, 450008, Henan Province, China

ARTICLE INFO

Keywords:
Breast cancer
Radiomics
Human epithelial growth factor receptor 2
Multiparametric MRI

ABSTRACT

Purpose: To investigate the potential of radiomics signatures (RSs) from intratumoral and peritumoral regions on multiparametric magnetic resonance imaging (MRI) to noninvasively evaluate HER2 status in breast cancer.

Method: In this retrospective study, 992 patients with pathologically confirmed breast cancers who underwent preoperative MRI were enrolled. The breast cancer lesions were segmented manually, and the intratumor region of interest (ROI_{Intra}) was dilated by 2, 4, 6 and 8 mm ($ROI_{Peri2mm}$, $ROI_{Peri4mm}$, $ROI_{Peri6mm}$, and $ROI_{Peri8mm}$, respectively). Quantitative radiomics features were extracted from dynamic contrast-enhanced T1-weighted imaging (DCE-T1), fat-saturated T2-weighted imaging (T2) and diffusion-weighted imaging (DWI). A three-step procedure was performed for feature selection, and RSs were constructed using a support vector machine (SVM) to predict HER2 status.

Result: The best single-area RSs for predicting HER2 status were DCE_Peri4mm-RS, T2_Peri4mm-RS, and DWI_Peri4mm-RS, yielding areas under the curve (AUCs) of 0.716 (95% confidence interval (CI), 0.648–0.778), 0.706 (95% CI, 0.637–0.768), and 0.719 (95% CI, 0.651–0.780), respectively, in the test set. The optimal RSs combining intratumoral and peritumoral regions for evaluating HER2 status were DCE-T1_Intra + DCE_Peri4mm-RS, T2_Intra + T2_Peri6mm-RS and DWI_Intra + DWI_Peri4mm-RS, with AUCs of 0.752 (95% CI, 0.686–0.810), 0.754 (95% CI, 0.688–0.812) and 0.725 (95% CI, 0.657–0.786), respectively, in the test set. Combining three sequences in the ROI_{Intra}, $ROI_{Peri2mm}$, $ROI_{Peri4mm}$, $ROI_{Peri6mm}$ and $ROI_{Peri8mm}$ areas, the optimal RS was DCE-T1_Peri4mm + T2_Peri4mm + DWI_Peri4mm-RS, achieving an AUC of 0.795 (95% CI, 0.733–0.849) in the test set.

* Corresponding author.
** Corresponding author.
E-mail addresses: zj360567346@sina.com (J. Zhou), yx_hnsrmyy@yeah.net (X. Yu), qx_wu1487@sina.com (Q. Wu), ypwu@ha.edu.cn (Y. Wu), fucongcong91@163.com (C. Fu), yx_wang1254@sina.com (Y. Wang), ml_hai7458@sina.com (M. Hai), natan2000@126.com (H. Tan), mywang@zzu.edu.cn (M. Wang).
[1] Lead contact.
[2] Contributed equally to this work.

https://doi.org/10.1016/j.heliyon.2024.e28722
Received 27 March 2023; Received in revised form 18 March 2024; Accepted 22 March 2024
Available online 4 April 2024

Conclusion: This study systematically explored the influence of the intratumoral region, different peritumoral sizes and their combination in radiomics analysis for predicting HER2 status in breast cancer based on multiparametric MRI and found the optimal RS.

1. Background

Breast cancer is the most common malignant tumor in women worldwide and remains the leading cause of female cancer-related death [1]. Breast cancer is a heterogeneous disease that exhibits different phenotypes and distinctive biological behaviors [2]. Slamon first reported that human epidermal growth factor receptor 2 (HER2) was one of the primary molecular treatment targets in patients with breast cancer in 1987 [3]. HER2 protein overexpression or gene amplification occurs in approximately 15%–20% of all breast cancers [4]. HER2-positive breast cancers tend to have accelerated growth and division of tumor cells and stimulated cell proliferation and angiogenesis, resulting in tumor heterogeneity [5]. With the development of anti-HER2 targeted therapies, the prognosis of patients with HER2-positive breast cancer has substantially improved. On the one hand, HER2-positive breast cancers exhibit good responses and high pathological complete response (pCR) rates after neoadjuvant chemotherapy with anti-HER2 antibodies (trastuzumab and pertuzumab), and these patients exhibit an obvious improvement in both disease-free survival and overall survival [6,7]. On the other hand, presurgical implementation of HER2 receptor–targeted monoclonal antibodies reduces the tumor burden and permits minimally invasive breast cancer resection in place of mastectomy in patients with a reduced tumor size [8]. Therefore, evaluation of the HER2 status of patients with breast cancer before surgery is crucial for personalized treatment.

Gene expression profiling or immunohistochemical (IHC) surrogates from invasive tissue sampling is the main method for evaluating the molecular subtypes of breast cancer to guide treatment selection [9]. However, a single biopsy of a potentially heterogeneous tumor acquires only a small part of the tumor tissue, resulting in selection bias instead of being completely representative of the genetic, epigenetic, and/or phenotypic changes of the entire tumor [10]. The recent literature [11–13] and our previous studies [14,15] suggest that radiomics signatures (RSs) based on medical images may help to predict the HER2 status of breast cancer, which improves the understanding of proteogenomics and its relation to cancer. However, most previous studies on the radiomics of breast cancer based on MRI focused on intratumoral areas or fixed peritumoral regions. Tumor evolution and progression are influenced by the interactions between intratumoral cells and peritumoral elements [16]. A previous study suggested that tumors consist of not only tumor cells but also stromal cells, such as cancer-associated fibroblasts, which cause significant alterations in the surrounding stroma, leading to a microenvironment that promotes tumor development [17]. Physical and genetic alterations within the peritumoral stroma help dictate the tumor's ability to grow and spread, escape the body's immune defenses, and resist therapeutic intervention [18], while

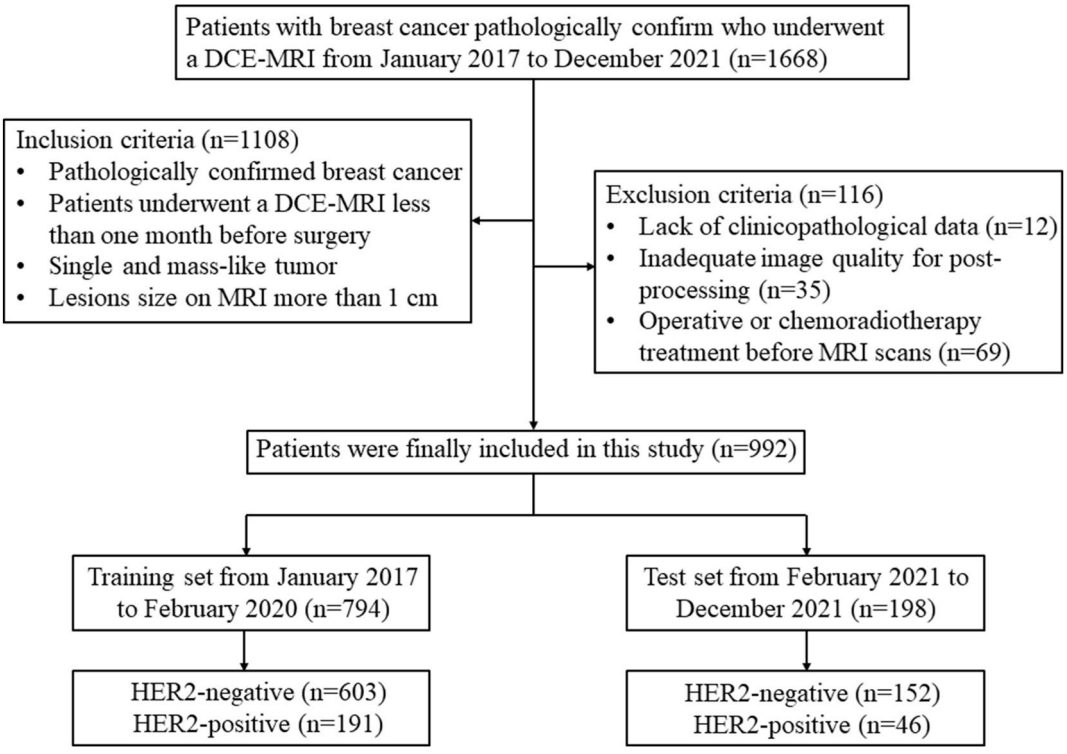

Fig. 1. Subject selection flowchart for this experiments.

the tumor necrosis factor signaling pathway, which is related to oncogenic angiogenesis, invasion, and metastasis, is correlated with peritumoral features [19]. Tchou et al. [20] reported that there were significant differences in the expression profiles of cancer-associated fibroblasts between the HER2-positive subtype and other subtypes of breast cancer. Therefore, both intratumoral and peritumoral areas of the tumor may contain some key biological information and potential predictive markers.

In this study, RSs based on the intratumoral area, different peritumoral areas, and combined regions or sequences were developed and validated for evaluating HER2 status in breast cancer. We then aimed to determine the optimal RSs for predicting HER2 status in breast cancer based on a single region of a single sequence, a combination of intratumoral and peritumoral areas in a single sequence and a combination of different sequences in intratumoral or peritumoral regions.

2. Materials and methods

2.1. Patient population

The Ethics Committee of Henan Provincial People's Hospital approved this study (NO. 2022-124), and the consent requirement were acquired from all subjects prior to enrollment in the study. In total, 1668 potentially eligible patients diagnosed by clinical examination and pathologically confirmed to have invasive breast cancer in our institution were retrospectively included in this study from January 2017 to December 2021. The patient inclusion criteria were as follows: (1) the diagnosis of invasive breast cancer was pathologically confirmed; (2) a multiparametric MRI scan was performed <1 month before surgery; (3) patients had a solitary mass-like tumor; and (4) to decrease the analytical influence of the partial volume effect on radiomics [21], the lesion size on MRI was ≥1 cm. The patient exclusion criteria were as follows: (1) incomplete clinical or pathological data; (2) inadequate image quality for postprocessing of multiparametric MRI; and (3) operative or chemoradiotherapy treatment before MRI scans. Ultimately, we included 992 women who met the criteria in this study. All enrolled patients were sorted in chronological order: the first 4/5 of patients (794 patients) comprised the training set, and the last 1/5 of patients (198 patients) comprised the test set. The flowchart of the patient recruitment process in our study is presented in Fig. 1.

2.2. Image acquisition

All breast MRI examinations were implemented using a 3.0 T (T) MR scanner (GE Medical Systems Discovery MR750, Milwaukee, WI) with a dedicated 8-channel breast phased-array coil from the same vendor. The MRI protocol included a non–fat-saturated T1-weighted sequence in the axial orientation, a non–fat-saturated T2-weighted sequence in the axial orientation, a fat-saturated T2-weighted sequence (hereafter T2) in the axial orientation, diffusion-weighted imaging (DWI) in the axial orientation and dynamic contrast-enhanced T1-weighted imaging (DCE-T1). The details of the parameters are shown in Supplementary Appendix 1.

2.3. Intratumoral segmentation, peritumoral dilation and feature extraction

The DCE-T1 (Phase 3), T2 and DWI (b value, 1000 s/mm^2) image data in DICOM format were imported into the publicly available software package ITK-SNAP (version 3.8.0, www.itksnap.org, University of Utah, Salt Lake City, UT, USA; University of Pennsylvania, Philadelphia, PA, USA). The region of interest (ROI) of entire lesions (avoiding cystic and necrotic areas), defined as ROI_{Intra}, was manually segmented by two experienced radiologists (more than 15 and 10 years of radiological diagnosis) who were blinded to the clinicopathological information of the patients. When a discrepancy of ≥5% between the ROIs delineated by the two radiologists occurred, a third radiologist with twenty years of experience performed ROI segmentation again and determined the final ROI. Then, the original data and ROIs of DCE-T1, T2 and DWI were uploaded to uAI Research Portal software (United Imaging Intelligence, China) for peritumoral ROI dilation, feature extraction and model construction. To further compare the intratumoral and peritumoral information, ROI_{Intra} was dilated by k mm (k = 2, 4, 6, and 8) (defined as $ROI_{k\ mm}$) using standard image morphological dilation operations. The intersection region between $ROI_{k\ mm}$ (k = 2, 4, 6, and 8) and ROI_{Intra} was defined as the peritumoral region ($ROI_{Peri\ k\ mm}$, k = 2, 4, 6, and 8). The $ROI_{Peri\ k\ mm}$ excluded skin, air, and pectoralis muscles. The uAI Research Portal software with the built-in package PyRadiomics (https://pyradiomics.readthedocs.io/en/latest/index.html) was used to perform feature extraction from the ROI_{Intra}, $ROI_{Peri2mm}$, $ROI_{Peri4mm}$, $ROI_{Peri6mm}$, and $ROI_{Peri8mm}$ areas from DCE-T1, T2 and DWI. The details of the radiomics features are described in Supplementary Appendix 2 and Tables S1–2.

2.4. Feature selection and model construction

The extracted features were standardized by using z score calculation with a mean of 0 and a standard deviation of 1 to prevent dependence on any individual feature, especially the parameters with high values. Feature selection is a method of reducing the large number of features acquired to the most relevant feature set and is based on the selection of certain features according to given mathematical criteria. Feature selection was conducted in the training set-based intratumoral area (ROI_{Intra}), peritumoral regions ($ROI_{Peri\ k\ mm}$, k = 2, 4, 6, and 8) and their combination on T2, DWI and DCE-T1 imaging. To identify the potential predictive radiomic features and avoid overfitting, we used the Mann–Whitney U test to select the significant features, followed by the chi-square test to select the top k significant features. Finally, least absolute shrinkage and selection operator (LASSO) was used to identify the features that had the most useful predictive value. According to these selected feature sets, the support vector machine (SVM) machine learning method was used to construct models for evaluating HER2 status in breast cancer. The performance of each model was assessed using

receiver operating characteristic (ROC) curves, and the area under the ROC curve (AUC), specificity and sensitivity were calculated. The radiomics flowchart of our study is presented in Fig. 2.

2.5. Pathological analysis

Pathological diagnosis by a pathologist with more than 20 years of experience was made based on postoperative tissue specimens or more than three tumor tissue samples acquired by breast biopsy. The specimens were fixed with formalin, embedded in paraffin and stained with hematoxylin and eosin (H&E). IHC analysis was used to define ER, PR, HER2, and Ki-67 expression. For ER and PR status, positivity was defined as ≥1% of tumor cells with positively stained nuclei. For HER2 status, positivity was defined as an IHC score of 3+, while negativity was defined as an IHC score of 0 or 1+. An IHC score of 2+ for HER2 was considered equivocal expression. Fluorescence in situ hybridization (FISH) was used to evaluate gene amplification, and HER2 positivity was considered if the ratio was ≥2.0. The IHC results of Ki-67 were defined as low expression (Ki-67 < 20%) or high expression (Ki-67 ≥ 20%). The histopathological grade was evaluated in accordance with the Nottingham Grading Score (NGS) [22]. This scoring system assesses tubule formation, pleomorphism, and mitotic count, and the total numerical score ranges from 3 to 9. Scores of 3–5 were classified as Grade 1 (G1), a score of 6 or 7 was classified as Grade 2 (G2), and a score of 8 or 9 was classified as Grade 3 (G3).

2.6. Statistical analysis

The baseline data of the patients were statistically analyzed using IBM SPSS, Version 22.0.0 (IBM Corp, Armonk, NY, USA). The qualitative data are presented as frequencies and percentages, while the quantitative data are presented as the mean ± SD. The differences in the qualitative data between the HER2-positive group and the HER2-negative group in the training set and test set were analyzed using the chi-square test, while the differences in the quantitative data were evaluated using Student's *t*-test or the Mann–Whitney *U* test on the basis of whether the data conformed to a normal distribution. The Delong test was used to compare the difference in AUCs between different models in the training and test sets. Two-sided p values ≤ 0.05 were considered statistically significant.

3. Results

3.1. Demographic characteristics

The clinical and histopathological characteristics of the patients in the HER2-positive and HER2-negative groups in the training and test sets are presented in Table 1. A total of 992 female patients with primary invasive ductal breast carcinoma were ultimately enrolled. The prevalence rates of HER2 positivity were 24.1% (192 of 794) and 23.2% (46 of 198) in the training and test sets, respectively. There was no significant difference in the mean age between the HER2-negative and HER2-positive groups (P = 0.828 and 0.192) in either the training or test sets. Significant differences in some clinicopathologic features in both the training and test sets were detected between the HER2-negative and HER2-positive groups, including histological grade, pathological ALN, ER and PR (all P < 0.05). There were significant differences in the mean diameter and Ki-67 expression in the training set (P = 0.001 and P < 0.001,

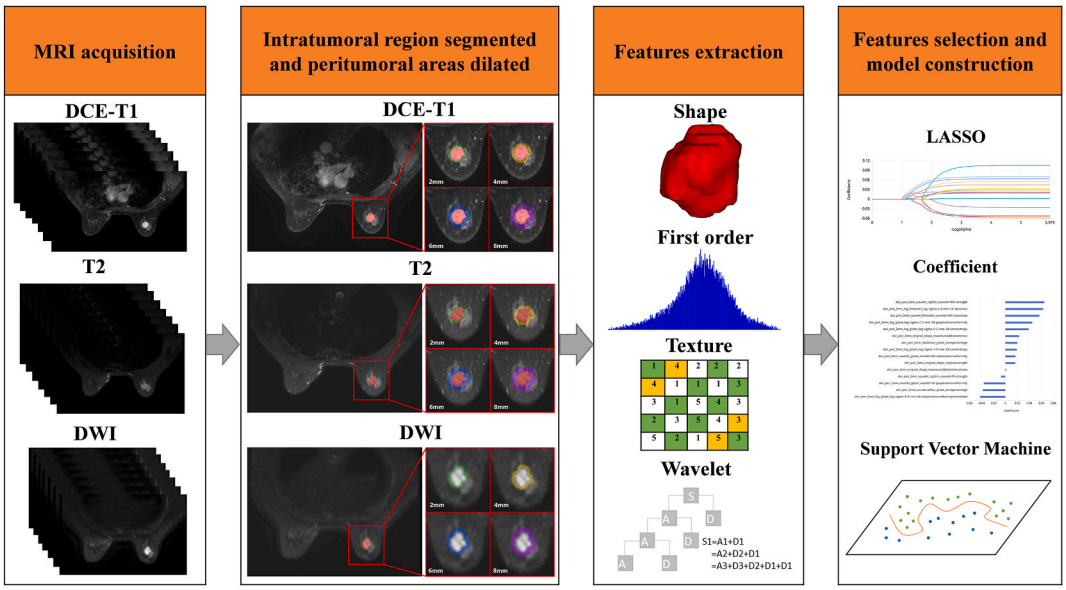

Fig. 2. The workflow of radiomics analysis.

Table 1
Clinical and histopathological characteristics of patients with breast cancer in the training and test sets.

Clinicopathological features	Training set (n = 794)		P	Test set (*n* = 198)		P
	HER2-(n = 602)	HER2+ (n = 192)		HER2-(n = 152)	HER2+ (n = 46)	
Age (years, mean ± SD)	48.88 ± 10.57	48.69 ± 9.63	0.828	48.94 ± 11.01	51.30 ± 9.85	0.192
Diameter (mm, mean ± SD)	24.47 ± 13.01	28.07 ± 14.54	**0.001**	24.18 ± 11.86	25.54 ± 9.85	0.195
Histological grade			**0.001**			**<0.001**
Low	19 (3.2%)	0		10 (6.6%)	0	
Moderate	407 (67.6%)	113 (58.9%)		116 (76.3%)	19 (41.3%)	
High	176 (29.2%)	79 (41.1%)		26 (17.1%)	27 (58.7%)	
Pathological ALN status			**<0.001**			**0.039**
Negative	409 (67.9%)	100 (52.1%)		116 (76.3%)	28 (60.9%)	
Positive	193 (32.1%)	92 (47.9%)		36 (23.7%)	18 (39.1%)	
ER			**<0.001**			**0.004**
Negative	130 (21.6%)	83 (43.2%)		28 (18.4%)	18 (39.1%)	
Positive	472 (78.4%)	109 (56.8%)		124 (81.6%)	28 (60.9%)	
PR			**<0.001**			**<0.001**
Negative	205 (34.1%)	118 (61.5%)		41 (27%)	26 (56.5%)	
Positive	397 (65.9%)	74 (38.5%)		111 (73%)	20 (43.5%)	
Ki-67 index (%)			**<0.001**			0.054
<20	185 (30.7%)	19 (9.9%)		60 (39.5%)	11 (23.9%)	
≥20	417 (69.3%)	193 (90.1%)		92 (60.5%)	35 (76.1%)	

HER2, human epidermal growth factor receptor 2; ALN, axillary lymph node; SD, standard deviation; ER, estrogen receptor; PR, progesterone receptor.

respectively) but not in the test set (P = 0.195 and P = 0.054, respectively).

3.2. Feature extraction, selection, and modeling

After eliminating redundant features by applying the Mann–Whitney *U* test, select k-best and LASSO in the training set, the selected feature sets based on ROI_{Intra} and $ROI_{Peri\ k\ mm}$ (k = 2, 4, 6, and 8) of DCE-T1, T2, and DWI were used to construct 15 RSs. We performed the same methods of feature selection to develop 32 combined RSs based on different regions and/or sequences. The steps and details of the selected features of each RS are presented in Tables S3–4.

3.3. Predictive performance of RSs

Tables 2–4 and Fig. 3A–F presents the performance for predicting HER2 status of single or combined RSs built with the ROI_{Intra}, $ROI_{Peri2mm}$, $ROI_{Peri4mm}$, $ROI_{Peri6mm}$, and $ROI_{Peri8mm}$ of DCE-T1, T2 and DWI. Based on these regions of DCE-T1, T2 and DWI, the optimal single-area RSs for the evaluation of HER2 status were DCE_Peri4mm-RS, T2_Peri4mm-RS, and DWI_Peri4mm-RS, with AUCs of 0.716 (95% confidence interval [CI], 0.648–0.778), 0.706 (95% CI, 0.637–0.768), and 0.719 (95% CI, 0.651–0.780), respectively, in the test set. There was a significant difference between the partial AUCs of single-area RSs in the training set (all $P < 0.05$), but there was no significant difference between all AUCs for single-area RSs in the test set (all $P > 0.05$). The details of the comparison are presented in Tables S5–6. Among the combinations of the ROI_{Intra} and $ROI_{Peri2mm}$, ROI_{Intra} and $ROI_{Peri4mm}$, ROI_{Intra} and $ROI_{Peri6mm}$ or ROI_{Intra} and

Table 2
Performance of intratumoral and peritumoral RSs of different sequences for evaluation of HER2 status.

RSs	Training Set (n = 794)			Test Set (n = 198)		
	AUC (95% CI)	SEN (%)	SPE (%)	AUC (95% CI)	SEN (%)	SPE (%)
DCE-T1_Intra-RS1	0.834 (0.806–0.859)	75.9	85.2	0.688 (0.618–0.752)	73.9	57.8
DCE-T1_Peri2mm-RS2	0.752 (0.720–0.781)	65.9	71.9	0.689 (0.619–0.752)	54.3	77.6
DCE-T1_Peri4mm-RS3	0.734 (0.702–0.765)	56.0	79.1	0.716 (0.648–0.778)	60.8	75.0
DCE-T1_Peri6mm-RS4	0.780 (0.750–0.809)	74.3	70.3	0.694 (0.624–0.757)	60.8	72.3
DCE-T1_Peri8mm-RS5	0.782 (0.751–0.810)	70.6	71.6	0.677 (0.607–0.742)	78.2	51.3
T2_Intra-RS6	0.807 (0.778–0.834)	58.1	89.2	0.641 (0.570–0.708)	89.1	34.8
T2_Peri2mm-RS7	0.768 (0.737–0.797)	61.2	78.6	0.673 (0.603–0.738)	86.9	42.1
T2_Peri4mm-RS8	0.787 (0.757–0.815)	63.3	83.4	0.706 (0.637–0.768)	69.5	68.4
T2_Peri6mm-RS9	0.759 (0.728–0.789)	64.9	73.4	0.657 (0.586–0.723)	45.6	79.6
T2_Peri8mm-RS10	0.748 (0.716–0.778)	67.0	70.9	0.694 (0.625–0.757)	56.5	73.6
DWI_Intra-RS11	0.683 (0.649–0.715)	62.3	69.1	0.649 (0.578–0.716)	73.9	54.6
DWI_Peri2mm-RS12	0.776 (0.746–0.805)	70.6	71.1	0.704 (0.635–0.766)	78.2	57.2
DWI_Peri4mm-RS13	0.725 (0.692–0.755)	62.3	75.1	0.719 (0.651–0.780)	65.2	77.6
DWI_Peri6mm-RS14	0.771 (0.740–0.800)	62.3	79.4	0.710 (0.641–0.772)	63.0	73.0
DWI_Peri8mm-RS15	0.785 (0.755–0.813)	70.6	74.1	0.708 (0.639–0.770)	71.7	64.4

RS, radiomics signature; AUC, area under the curve; CI, confidence interval; SEN, sensitivity; SPE, specificity; ACC, accuracy.

Table 3
Performance of RSs combining intratumoral and peritumoral regions of different sequences for evaluation of HER2 status.

RSs	Training Set (n = 794)			Test Set (n = 198)		
	AUC (95% CI)	SEN (%)	SPE (%)	AUC (95% CI)	SEN (%)	SPE (%)
DCE-T1_Intra + DCE_Peri2mm-RS1	0.808 (0.779–0.835)	72.2	78.9	0.725 (0.657–0.786)	67.3	71.7
DCE-T1_Intra + DCE_Peri4mm-RS2	0.797 (0.768–0.825)	60.2	87.2	0.752 (0.686–0.810)	73.9	65.1
DCE-T1_Intra + DCE_Peri6mm-RS3	0.843 (0.816–0.868)	73.3	81.4	0.716 (0.647–0.777)	56.5	78.9
DCE-T1_Intra + DCE_Peri8mm-RS4	0.836 (0.809–0.861)	76.9	76.6	0.730 (0.662–0.790)	69.5	63.8
T2_Intra + T2_Peri2mm-RS5	0.867 (0.841–0.890)	81.1	78.2	0.727 (0.660–0.788)	65.2	71.0
T2_Intra + T2_Peri4mm-RS6	0.874 (0.849–0.897)	83.7	77.4	0.747 (0.680–0.806)	71.7	69.0
T2_Intra + T2_Peri6mm-RS7	0.849 (0.822–0.873)	73.3	83.0	0.754 (0.688–0.812)	86.9	55.2
T2_Intra + T2_Peri8mm-RS8	0.859 (0.833–0.882)	82.2	77.6	0.735 (0.668–0.795)	93.4	44.0
DWI_Intra + DWI_Peri2mm-RS9	0.717 (0.684–0.748)	61.2	74.9	0.715 (0.646–0.776)	63.0	76.3
DWI_Intra + DWI_Peri4mm-RS10	0.770 (0.739–0.799)	56.0	85.7	0.725 (0.657–0.786)	71.7	69.7
DWI_Intra + DWI_Peri6mm-RS11	0.793 (0.763–0.820)	69.1	75.6	0.723 (0.656–0.785)	58.7	76.3
DWI_Intra + DWI_Peri8mm-RS12	0.799 (0.769–0.826)	74.3	75.9	0.713 (0.644–0.775)	80.4	53.9

RS, radiomics signature; AUC, area under the curve; CI, confidence interval; SEN, sensitivity; SPE, specificity; ACC, accuracy.

Table 4
Performance of RSs combining different sequences in intratumoral or peritumoral regions for evaluating HER2 status.

RSs	Training Set (n = 794)			Test Set (n = 198)		
	AUC (95% CI)	SEN (%)	SPE (%)	AUC (95% CI)	SEN (%)	SPE (%)
DCE-T1_Intra + T2_Intra-RS1	0.844 (0.817–0.869)	72.2	83.2	0.738 (0.671–0.798)	89.1	51.9
DCE-T1_Intra + DWI_Intra-RS2	0.809 (0.780–0.836)	77.4	72.4	0.728 (0.660–0.789)	80.4	59.2
T2_Intra + DWI_Intra-RS3	0.829 (0.801–0.854)	76.9	77.9	0.730 (0.662–0.790)	91.3	48.0
DCE-T1_Intra + T2_Intra + DWI_Intra-RS4	0.866 (0.841–0.889)	75.3	83.2	0.760 (0.694–0.817)	69.5	71.7
DCE-T1_Peri2mm + T2_Peri2mm-RS5	0.826 (0.798–0.852)	69.6	81.2	0.753 (0.687–0.811)	67.3	75.0
DCE-T1_Peri2mm + DWI_Peri2mm-RS6	0.804 (0.775–0.831)	76.4	72.3	0.758 (0.692–0.816)	63.0	77.6
T2_Peri2mm + DWI_Peri2mm-RS7	0.822 (0.793–0.848)	75.9	70.1	0.782 (0.718–0.838)	78.2	61.8
DCE-T1_Peri2mm + T2_Peri2mm + DWI_Peri2mm-RS8	0.848 (0.822–0.873)	79.5	75.6	0.787 (0.723–0.842)	80.4	62.5
DCE-T1_ Peri4mm + T2_ Peri4mm-RS9	0.832 (0.804–0.857)	68.5	82.4	0.744 (0.677–0.803)	78.2	65.7
DCE-T1_Peri4mm + DWI_Peri4mm-RS10	0.817 (0.788–0.843)	76.9	73.8	0.756 (0.690–0.814)	69.5	70.3
T2_Peri4mm + DWI_Peri4mm-RS11	0.833 (0.805–0.858)	73.3	79.7	0.752 (0.685–0.810)	84.7	55.9
DCE-T1_Peri4mm + T2_Peri4mm + DWI_Peri4mm-RS12	0.868 (0.842–0.890)	83.7	72.8	0.795 (0.733–0.849)	80.4	69.7
DCE-T1_Peri6mm + T2_Peri6mm-RS13	0.848 (0.821–0.873)	79.5	75.2	0.742 (0.675–0.802)	82.6	58.5
DCE-T1_Peri6mm + DWI_Peri6mm-RS14	0.830 (0.802–0.856)	72.2	76.9	0.733 (0.665–0.793)	65.2	73.0
T2_Peri6mm + DWI_Peri6mm-RS15	0.829 (0.801–0.854)	66.4	82.2	0.737 (0.669–0.796)	73.9	63.8
DCE-T1_Peri6mm + T2_Peri6mm + DWI_Peri6mm-RS16	0.870 (0.844–0.892)	70.6	86.2	0.774 (0.709–0.830)	65.2	79.6
DCE-T1_Peri8mm + T2_Peri8mm-RS17	0.854 (0.827–0.877)	84.2	72.8	0.702 (0.633–0.765)	80.4	51.3
DCE-T1_Peri8mm + DWI_Peri8mm-RS18	0.828 (0.800–0.854)	70.6	80.9	0.739 (0.672–0.798)	71.7	67.7
T2_Peri8mm + DWI_Peri8mm-RS19	0.862 (0.836–0.885)	83.2	74.1	0.763 (0.698–0.820)	91.3	51.3
DCE-T1_Peri8mm + T2_Peri8mm + DWI_Peri8mm-RS20	0.811 (0.782–0.838)	70.6	79.1	0.777 (0.713–0.833)	76.0	71.7

RS, radiomics signature; AUC, area under the curve; CI, confidence interval; SEN, sensitivity; SPE, specificity; ACC, accuracy.

$ROI_{Peri8mm}$ regions of DCE-T1, T2 and DWI, DCE-T1_Intra + DCE_Peri4mm-RS, T2_Intra + T2_Peri6mm-RS and DWI_Intra + DWI_-Peri4mm-RS were the best RSs to predict HER2 status, achieving AUCs of 0.752 (95% CI, 0.686–0.810), 0.754 (95% CI, 0.688–0.812) and 0.725 (95% CI, 0.657–0.786), respectively, in the test set. The differences in partial AUCs of combined intra- and peritumoral RSs in the training set were significant (all $P < 0.05$), while the differences in all AUCs of combined intra- and peritumoral RSs in the test set were not significant (all $P > 0.05$). The details of the comparison are shown in Tables S7–8. Among the combinations of DCE-T1 and T2, DCE-T1 and DWI, or T2 and DWI of the ROI_{Intra}, $ROI_{Peri2mm}$, $ROI_{Peri4mm}$, $ROI_{Peri6mm}$ and $ROI_{Peri8mm}$ regions, the optimal RSs of double sequences to evaluate HER2 status were DCE-T1_Intra + T2_Intra-RS, T2_Peri2mm + DWI_Peri2mm-RS, DCE-T1_Peri4mm + DWI_-Peri4mm-RS, DCE-T1_Peri6mm + T2_Peri6mm-RS, and T2_Peri8mm + DWI_Peri8mm-RS, yielding AUCs of 0.738 (95% CI, 0.671–0.798), 0.782 (95% CI, 0.718–0.838), 0.756 (95% CI, 0.690–0.814), 0.742 (95% CI, 0.675–0.802) and 0.763 (95% CI, 0.713–0.833), respectively, in the test set. Among the combined three sequences of the ROI_{Intra}, $ROI_{Peri2mm}$, $ROI_{Peri4mm}$, $ROI_{Peri6mm}$ and $ROI_{Peri8mm}$ regions, the optimal RS was DCE-T1_Peri4mm + T2_Peri4mm + DWI_Peri4mm-RS, with an AUC of 0.795 (95% CI, 0.733–0.849) in the test set. The partially combined multimodal RSs in different regions were significant (all $P < 0.05$) in the training or test sets, and the details can be found in Tables S9–10.

4. Discussion

In this study, based on the tumoral region, peritumoral areas with different dilation distances and their combination from DCE-T1, T2 and DWI using multiparametric MRI, we developed and validated different RSs to evaluate HER2 status in patients with breast cancer by using machine learning methods. This investigation of the effect of peritumoral region sizes in breast cancer can help identify

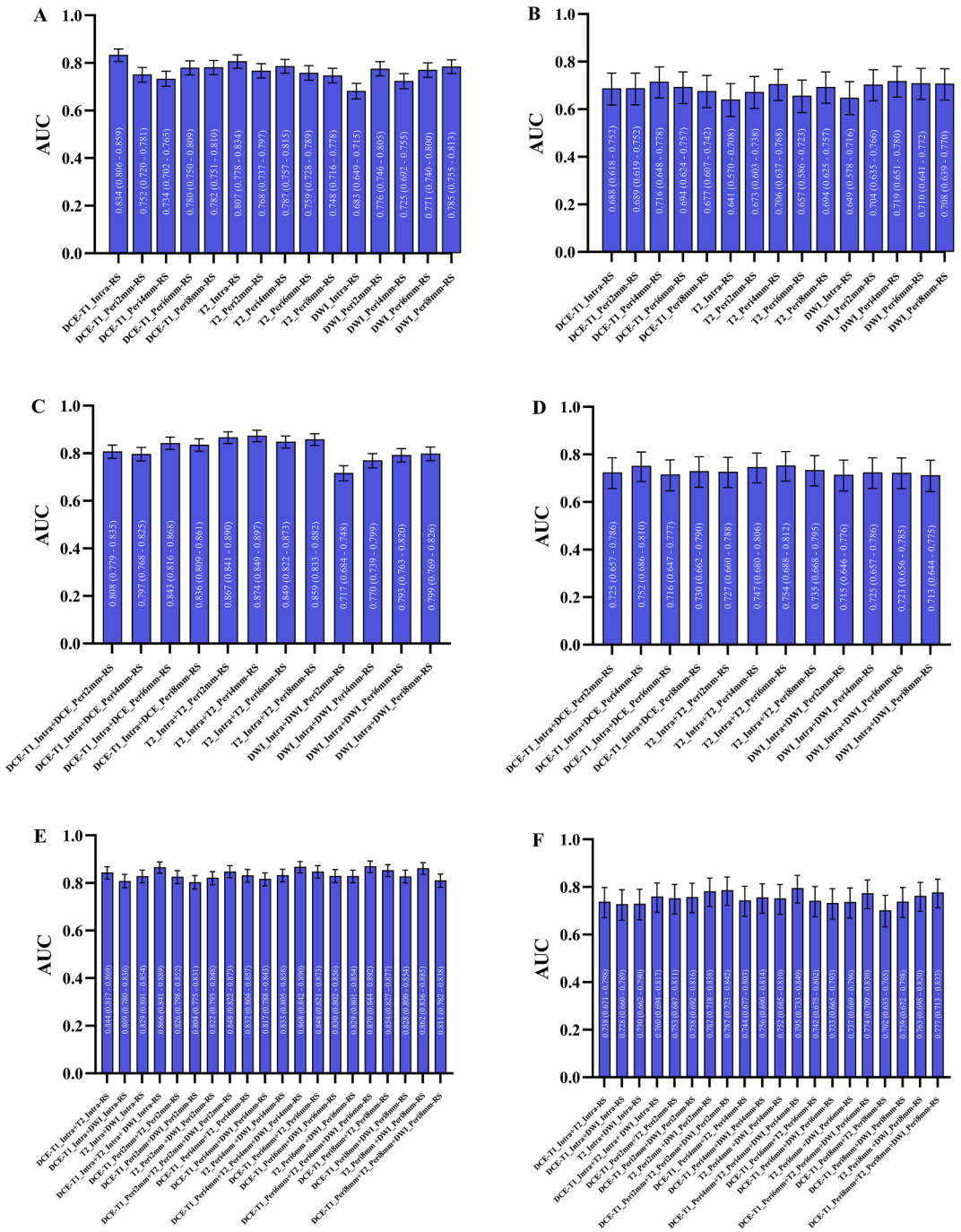

Fig. 3. The histogram presents the performance of different RSs for evaluating HER2 status of breast cancer.
The histograms were drawn to demonstrate the RSs performance of intratmoral or peritumoral radiomics features of different sequences (A–B), combining intratmoral and peritumoral radiomics features from different sequences (C–D) and combining different sequences radiomics features in intratumoral or peritumoral regions (E–F) in the training and test sets, respectively.

the optimal areas of a single sequence and the best combinations of regions in a single sequence or across different sequences in which radiomics features can achieve the best performance for predicting HER2 status in breast cancer.

We first developed and validated single RSs for the evaluation of HER2 status in breast cancer built based on the ROI_{Intra}, $ROI_{Peri2mm}$, $ROI_{Peri4mm}$, $ROI_{Peri6mm}$ and $ROI_{Peri8mm}$ regions from DCE-T1, T2 and DWI. The results showed that the best single RSs for the prediction of HER2 status were DCE_Peri4mm-RS, T2_Peri4mm-RS, and DWI_Peri4mm-RS, achieving AUCs of 0.716, 0.706, and 0.719, respectively, in the test set. This finding identifies the optimal regions to use to evaluate HER2 status according to a single sequence.

This result also suggests that radiomics features extracted from peritumoral areas dilated by 4 mm have superior performance in evaluating HER2 status in breast cancer. This observation was confirmed in the prediction of sentinel lymph node status in breast cancer. Ding et al. [23] compared radiomics analysis for the predictive performance of sentinel lymph node status of breast cancer in different peritumoral region sizes, including 0 mm, 2 mm, 4 mm, 6 mm, and 8 mm, and found that a peritumoral thickness of 4 mm had the optimal predictive performance. The reason for differences in RS performances at different peritumoral thicknesses may be associated with the immune microenvironment characteristics of breast cancer. The proximal peritumoral areas have higher immune cell densities than the intratumoral and distal peritumoral regions [24]. To explore the optimal peritumoral thickness to improve the performance of RSs for evaluating HER2 status in patients with breast cancer, we combined peritumoral regions of different sizes with intratumoral areas to determine the best combinations. Our findings indicate that DCE-T1_Intra + DCE_Peri4mm-RS, T2_Intra + T2_Peri6mm-RS and DWI_Intra + DWI_Peri4mm-RS were promising for predicting HER2 status, with AUCs of 0.752, 0.754 and 0.725, respectively, in the test set. These results not only confirm the usefulness of peritumoral features in RSs but also demonstrate that the selection of the peritumoral size influences the prediction results of the RSs. Thus, uncertain or arbitrary peritumoral area thicknesses should not be used in radiomics studies with peritumoral features. In contrast, it is recommended that the best peritumoral sizes be defined based on systematic comparison to optimize the predictive models and improve their efficiency.

The peritumoral environment is related to the tumoral process of neoangiogenesis, which may lead to increased vascular permeability in the newly formed vessels and the secretion of peritumoral cytokines, playing important roles in tumor development, progression and metastasis [22]. Combining tumor and peritumor data can more comprehensively portray the biological characteristics of tumors. Thus, extracting and fusing tumor and peritumor features can improve the predictive performance of radiomics models. The results of our study are consistent with those of some studies combining intratumoral and peritumoral areas. Li et al. [12] reported that radiomics models of the intratumoral region, peritumoral area and their combination based on functional parametric maps from breast DCE-MRI for the evaluation of HER2 and Ki-67 status yielded AUCs of 0.683, 0.690 and 0.713 in the test set for HER2 and AUCs of 0.714, 0.692, and 0.749 in the test set for Ki-67, respectively. Moreover, the theory that peritumoral radiomics features can provide extra value was also confirmed in treatment response prediction. A previous study conducted by Huang et al. [25] suggested that the intratumoral, peritumoral and combined intratumoral and peritumoral RSs for the prediction of pCR to neoadjuvant chemotherapy in breast cancer based on contrast-enhanced computed tomography (CECT) achieved AUCs of 0.728, 0.673 and 0.737, respectively, in the test set.

In addition to the improved efficiency of RSs for predicting HER2 status caused by combining intratumoral and peritumoral features, combining different sequences can also improve the predictive performance. In our previous study, we developed and validated three intratumoral RSs for distinguishing HER2-positive from HER2-negative breast cancer based on DCE-T1, T2 and their combination, with AUCs of 0.70, 0.68, and 0.81, respectively, in the test set. However, we had not explored the performance of the combination of different sequences in evaluating HER2 status in breast cancer with the ideal peritumoral thickness in our previous study. To comprehensively investigate the best combination to optimize the performance of RSs for predicting HER2 status in breast cancer, we compared the performance for predicting the HER2 status of RSs by combining different sequences based on the ROI_{Intra}, $ROI_{Peri2mm}$, $ROI_{Peri4mm}$, $ROI_{Peri6mm}$ and $ROI_{Peri8mm}$ regions. The best double-sequence RSs of these regions for assessing HER2 status were DCE-T1_Intra + T2_Intra-RS, T2_Peri2mm + DWI_Peri2mm-RS, DCE-T1_Peri4mm + DWI_Peri4mm-RS, DCE-T1_Peri6mm + T2_Peri6mm-RS, and T2_Peri8mm + DWI_Peri8mm-RS, with AUCs of 0.738, 0.782, 0.756, 0.742 and 0.763, respectively, in the test set. When we combined the three sequences for the peritumoral region expanded by 4 mm, the efficiency of predicting HER2 status achieved a maximum AUC of 0.795 in the test set. The Delong test reveals that there were significant difference (all $P < 0.05$) between the AUCs of optimal RS and partial double sequences RSs in test set. These results suggest that the RSs built by combining different sequences of different areas can also improve the performance of the evaluation of HER2 status in breast cancer.

We found that most of the selected features used in the RSs were shape-based, first-order statistics and gray-level size zone matrix (GLSZM) features. Shape-based features are external characteristics of the area that describe the shape, surface and size information of the ROIs (e.g., typical characteristics such as sphericity). First-order statistical features, such as the mean and median, represent the overall intensity and variation of the ROIs [26]. GLSZM features, which are rotation independent and appropriate for assessing heterogeneous and nonperiodic textures, describe tumor heterogeneity on a regional scale and homogeneous areas within the tumor volume [27]. The results of our study are consistent with those of some existing studies. Our previous study [14] suggested that some shape-based, first-order and GLSZM features (e.g., original_shape_Sphericity, wavelet-HHH_firstorder_mean and lbp-2D_glszm_ZoneEntropy) extracted from DCE-T1 or T2 were significantly associated with HER2 status in breast cancer. Xu et al. [28] reported that the top 11 features, including morphological, first-order, gray level dependence matrix (GLDM), gray-level cooccurrence matrix (GLCM) and GLSZM features, principally represented tumor heterogeneity (especially shape_Maximum 2D Diameter, shape_Maximum 3D Diameter, and shape_Sphericity), which is associated with HER2 expression in breast carcinoma. The usefulness of these features was also observed in a radiomics analysis of the mammographic 2D modality for predicting HER2 status in breast cancer. In our previous study [15], we developed and validated a noninvasive evaluation method of mammography RSs, including cranial caudal (CC) and mediolateral oblique (MLO) views, that showed efficacy in pathologically diagnosing breast cancer patients' HER2 status. In this study, we found some typical features with high efficiency, such as MLO_original_shape_Maximum2DDiameterRow, CC_original_first order_Energy and CC_original_glszm_SmallAreaLowGrayLevelEmphasis. Laws and Gabor features are also important in the evaluation of HER2 status in breast cancer. Gabor features can be used to comprehensively quantify the heterogeneity of tumors across different spatial scales at different directional orientations [29]. Laws features have a stronger capability to detect patterns of incongruent enhancement and abnormal structure generated by a robust immune response [30]. A recent study [12] reported that a combined RS constructed by 9 Gabor, 6 Laws and 4 GLCM features extracted from intratumoral and peritumoral regions of functional parametric maps derived from DCE-T1 exhibited optimal performance for predicting HER2 status.

RSs based on ultrasound [31], mammography [15], computed tomography [13], and ^{18}F-fluorodeoxyglucose positron emission tomography/computed tomography (^{18}F-FDG PET/CT) [11] can also show some predictive efficiency for HER2 status in breast cancer. Xu et al. [31] developed a 3-block-DenseNet–based deep learning model based on ultrasound images to evaluate HER2 status in patients with breast cancer and achieved AUCs of 0.87 in the training set and 0.84 in the test set. Our previous radiomics analysis of mammography [15] for predicting HER2 status showed good performance, with AUC and accuracy values of 0.84 and 80.0% in the training set and 0.787 and 73.9% in the testing set. Fan et al. [32] found that radiomics features extracted from multidetector computed tomography (MDCT) during the nonenhanced (NE), arterial phase (AP) and portal-venous phase (PVP) could be a promising tool to noninvasively evaluate HER2 expression in breast carcinoma; the combined model incorporating radiomics features of NE, AP and PVP presented an optimal discriminative ability, with an AUC of 0.881. Liu et al. [33] found that a machine learning model based on ^{18}F-FDG PET/CT can be used to predict HER2 expression in breast cancer, with an AUC of 0.818. However, few studies have comprehensively compared the predictive performance of intratumoral, peritumoral and combined RSs of different sequences for the evaluation of HER2 status in breast carcinoma. A more comprehensive comparative study with multimodal imaging and different peritumoral regions is necessary in the future to find the optimal model with high cost-effectiveness.

There were some limitations in our study. First, this retrospective and single-center study had inherent selection bias, although we enrolled a large sample size. External validation of the stability and clinical applicability of the model is needed in a multicenter dataset in the future. Second, the ROIs were delineated manually by radiologists, which was time-consuming and may have caused some inaccuracies because the judgment of the lesion boundary was greatly associated with the experience of the radiologist. Therefore, a standardized, automatic, repeatable and validated segmentation method would be ideal even if not yet available. Third, we only used DCE-T1, T2 and DWI sequences to construct RSs for predicting HER2 status in breast cancer because these sequences are most commonly obtainable in clinical practice.

5. Conclusion

In this study, we developed and validated single and combined RSs based on multiparametric MRI-based intratumoral regions and different peritumoral thicknesses that noninvasively predicted HER2 status in breast cancer before surgery. We identified the best single-area RSs of different sequences, the optimal RSs combining intratumoral and peritumoral regions, the best double-sequence RSs of different regions, and the optimum RS combining three sequences of different regions for predicting HER2 status in breast cancer. Our results indicate that peritumoral areas contain important information on tumor biological characteristics and that the prediction performance of RSs can be influenced by the size of the peritumoral region.

Ethics approval and consent to participate

The Research Ethics Committee of the Henan Provincial People's Hospital approved this retrospective study (NO. 2022-124) and the consent requirement were acquired from all subjects prior to enrollment in the study.

Images published statement

Participants consented to have these images published.

Funding statement

This work was supported by the Natural Science Foundation of Henan Province (No. 202300410081) and the Scientific and Technological Research Project of Henan Province (LHGJ20220056, LHGJ20220055, SBGJ202101002).

CRediT authorship contribution statement

Jing Zhou: Writing – review & editing, Writing – original draft, Software, Project administration, Methodology, Investigation, Funding acquisition, Formal analysis, Data curation, Conceptualization. **Xuan Yu:** Writing – original draft, Supervision, Software, Resources, Project administration, Methodology, Investigation, Formal analysis, Data curation. **Qingxia Wu:** Resources, Project administration, Methodology, Investigation, Formal analysis, Data curation. **Yaping Wu:** Supervision, Software, Resources, Project administration, Methodology, Formal analysis. **Cong Fu:** Supervision, Resources, Methodology, Investigation, Formal analysis, Data curation. **Yunxia Wang:** Methodology, Investigation, Formal analysis, Data curation. **Menglu Hai:** Methodology, Investigation, Formal analysis, Data curation. **Hongna Tan:** Writing – review & editing, Writing – original draft, Supervision, Software, Resources, Project administration, Methodology, Investigation, Funding acquisition, Formal analysis, Data curation. **Meiyun Wang:** Writing – review & editing, Writing – original draft, Supervision, Software, Resources, Project administration, Methodology, Investigation, Funding acquisition, Formal analysis, Data curation, Conceptualization.

Declaration of competing interest

The authors declare that they have no known competing financial interests or personal relationships that could have appeared to influence the work reported in this paper.

Appendix A. Supplementary data

Supplementary data to this article can be found online at https://doi.org/10.1016/j.heliyon.2024.e28722.

References

[1] K.D. Miller, L. Nogueira, T. Devasia, et al., Cancer treatment and survivorship statistics, 2022, CA Cancer J Clin 72 (5) (2022) 409–436, https://doi.org/10.3322/caac.21731.

[2] C.M. Perou, T. Sorlie, M.B. Eisen, et al., Molecular portraits of human breast tumours, Nature 406 (6797) (2000) 747–752, https://doi.org/10.1038/35021093.

[3] D.J. Slamon, G.M. Clark, S.G. Wong, et al., Human breast cancer: correlation of relapse and survival with amplification of the HER-2/neu oncogene, Science 235 (4785) (1987) 177–182, https://doi.org/10.1126/science.3798106.

[4] P. Sharma, Major strides in HER2 blockade for metastatic breast cancer, N. Engl. J. Med. 382 (7) (2020) 669–671, https://doi.org/10.1056/NEJMe1916310.

[5] R.A. Mohammed, I.O. Ellis, A.M. Mahmmod, et al., Lymphatic and blood vessels in basal and triple-negative breast cancers: characteristics and prognostic significance, Mod. Pathol. 24 (6) (2011) 774–785, https://doi.org/10.1038/modpathol.2011.4.

[6] A. Llombart-Cussac, J. Cortes, L. Pare, et al., HER2-enriched subtype as a predictor of pathological complete response following trastuzumab and lapatinib without chemotherapy in early-stage HER2-positive breast cancer (PAMELA): an open-label, single-group, multicentre, phase 2 trial, Lancet Oncol. 18 (4) (2017) 545–554, https://doi.org/10.1016/S1470-2045(17)30021-9.

[7] A. Prat, M.C. Cheang, P. Galvan, et al., Prognostic value of intrinsic subtypes in hormone receptor-positive metastatic breast cancer treated with letrozole with or without lapatinib, JAMA Oncol. 2 (10) (2016) 1287–1294, https://doi.org/10.1001/jamaoncol.2016.0922.

[8] L. Wiechmann, M. Sampson, M. Stempel, et al., Presenting features of breast cancer differ by molecular subtype, Ann. Surg Oncol. 16 (10) (2009) 2705–2710, https://doi.org/10.1245/s10434-009-0606-2.

[9] A. Prat, E. Pineda, B. Adamo, et al., Clinical implications of the intrinsic molecular subtypes of breast cancer, Breast 24 (Suppl 2) (2015) S26–S35, https://doi.org/10.1016/j.breast.2015.07.008.

[10] A.O. Pisco, S. Huang, Non-genetic cancer cell plasticity and therapy-induced stemness in tumour relapse: 'What does not kill me strengthens me', Br. J. Cancer 112 (11) (2015) 1725–1732, https://doi.org/10.1038/bjc.2015.146.

[11] Y. Chen, Z. Wang, G. Yin, et al., Prediction of HER2 expression in breast cancer by combining PET/CT radiomic analysis and machine learning, Ann. Nucl. Med. 36 (2) (2022) 172–182, https://doi.org/10.1007/s12149-021-01688-3.

[12] C. Li, L. Song, J. Yin, Intratumoral and peritumoral radiomics based on functional parametric maps from breast DCE-MRI for prediction of HER-2 and ki-67 status, J Magn Reson Imaging 54 (3) (2021) 703–714, https://doi.org/10.1002/jmri.27651.

[13] X. Yang, L. Wu, K. Zhao, et al., Evaluation of human epidermal growth factor receptor 2 status of breast cancer using preoperative multidetector computed tomography with deep learning and handcrafted radiomics features, Chin. J. Cancer Res. 32 (2) (2020) 175–185, https://doi.org/10.21147/j.issn.1000-9604.2020.02.05.

[14] J. Zhou, H. Tan, W. Li, et al., Radiomics signatures based on multiparametric MRI for the preoperative prediction of the HER2 status of patients with breast cancer, Acad. Radiol. 28 (10) (2021) 1352–1360, https://doi.org/10.1016/j.acra.2020.05.040.

[15] J. Zhou, H. Tan, Y. Bai, et al., Evaluating the HER-2 status of breast cancer using mammography radiomics features, Eur. J. Radiol. 121 (2019) 108718, https://doi.org/10.1016/j.ejrad.2019.108718.

[16] K. Kessenbrock, V. Plaks, Z. Werb, Matrix metalloproteinases: regulators of the tumor microenvironment, Cell 141 (1) (2010) 52–67, https://doi.org/10.1016/j.cell.2010.03.015.

[17] Z. Liu, M. Mi, X. Li, et al., A lncRNA prognostic signature associated with immune infiltration and tumour mutation burden in breast cancer, J. Cell Mol. Med. 24 (21) (2020) 12444–12456, https://doi.org/10.1111/jcmm.15762.

[18] N. Braman, P. Prasanna, J. Whitney, et al., Association of peritumoral radiomics with tumor biology and pathologic response to preoperative targeted therapy for HER2 (ERBB2)-Positive breast cancer, JAMA Netw. Open 2 (4) (2019) e192561, https://doi.org/10.1001/jamanetworkopen.2019.2561.

[19] F. Balkwill, TNF-alpha in promotion and progression of cancer, Cancer Metastasis Rev. 25 (3) (2006) 409–416, https://doi.org/10.1007/s10555-006-9005-3.

[20] J. Tchou, A.V. Kossenkov, L. Chang, et al., Human breast cancer associated fibroblasts exhibit subtype specific gene expression profiles, BMC Med Genomics 5 (2012) 39, https://doi.org/10.1186/1755-8794-5-39.

[21] D. Leithner, J.V. Horvat, M.A. Marino, et al., Radiomic signatures with contrast-enhanced magnetic resonance imaging for the assessment of breast cancer receptor status and molecular subtypes: initial results, Breast Cancer Res. 21 (1) (2019) 106, https://doi.org/10.1186/s13058-019-1187-z.

[22] D. Santucci, E. Faiella, E. Cordelli, et al., The impact of tumor edema on T2-weighted 3T-MRI invasive breast cancer histological characterization: a pilot radiomics study, Cancers 13 (18) (2021), https://doi.org/10.3390/cancers13184635.

[23] J. Ding, S. Chen, M. Serrano Sosa, et al., Optimizing the peritumoral region size in radiomics analysis for sentinel lymph node status prediction in breast cancer, Acad. Radiol. 29 (Suppl 1) (2022) S223–S228, https://doi.org/10.1016/j.acra.2020.10.015. Suppl 1.

[24] G. Griguolo, G. Serna, T. Pascual, et al., Immune microenvironment characterisation and dynamics during anti-HER2-based neoadjuvant treatment in HER2-positive breast cancer, npj Precis. Oncol. 5 (1) (2021) 23, https://doi.org/10.1038/s41698-021-00163-6.

[25] X. Huang, J. Mai, Y. Huang, et al., Radiomic nomogram for pretreatment prediction of pathologic complete response to neoadjuvant therapy in breast cancer: predictive value of staging contrast-enhanced CT, Clin. Breast Cancer 21 (4) (2021) e388–e401, https://doi.org/10.1016/j.clbc.2020.12.004.

[26] M. Avanzo, L. Wei, J. Stancanello, et al., Machine and deep learning methods for radiomics, Med. Phys. 47 (5) (2020) e185–e202, https://doi.org/10.1002/mp.13678.

[27] R. Fusco, A. Piccirillo, M. Sansone, et al., Radiomics and artificial intelligence analysis with textural metrics extracted by contrast-enhanced mammography in the breast lesions classification, Diagnostics 11 (5) (2021), https://doi.org/10.3390/diagnostics11050815.

[28] A. Xu, X. Chu, S. Zhang, et al., Development and validation of a clinicoradiomic nomogram to assess the HER2 status of patients with invasive ductal carcinoma, BMC Cancer 22 (1) (2022) 872, https://doi.org/10.1186/s12885-022-09967-6.

[29] N.M. Braman, M. Etesami, P. Prasanna, et al., Intratumoral and peritumoral radiomics for the pretreatment prediction of pathological complete response to neoadjuvant chemotherapy based on breast DCE-MRI, Breast Cancer Res. 19 (1) (2017) 57, https://doi.org/10.1186/s13058-017-0846-1.

[30] C. Liu, J. Ding, K. Spuhler, et al., Preoperative prediction of sentinel lymph node metastasis in breast cancer by radiomic signatures from dynamic contrast-enhanced MRI, J Magn Reson Imaging 49 (1) (2019) 131–140, https://doi.org/10.1002/jmri.26224.

[31] Z. Xu, Q. Yang, M. Li, et al., Predicting HER2 status in breast cancer on ultrasound images using deep learning method, Front. Oncol. 12 (2022) 829041, https://doi.org/10.3389/fonc.2022.829041.

[32] Y. Fan, X. Pan, F. Yang, et al., Preoperative computed tomography radiomics analysis for predicting receptors status and ki-67 levels in breast cancer, Am. J. Clin. Oncol. 45 (12) (2022) 526–533, https://doi.org/10.1097/COC.0000000000000951.

[33] J. Liu, H. Bian, Y. Zhang, et al., Molecular subtype classification of breast cancer using established radiomic signature models based on (18)F-FDG PET/CT images, Front Biosci (Landmark Ed) 26 (9) (2021) 475–484, https://doi.org/10.52586/4960.